# Multimodal SHG-2PF Imaging of Microdomain $Ca^{2+}$-Contraction Coupling in Live Cardiac Myocytes

Samir Awasthi, Leighton T. Izu, Ziliang Mao, Zhong Jian, Trevor Landas, Aaron Lerner, Rafael Shimkunas, Rahwa Woldeyesus, Julie Bossuyt, Brittani Wood, Yi-Je Chen, Dennis L. Matthews, Deborah K. Lieu, Nipavan Chiamvimonvat, Kit S. Lam, Ye Chen-Izu,* James W. Chan*

***Rationale:*** **Cardiac myocyte contraction is caused by $Ca^{2+}$ binding to troponin C, which triggers the cross-bridge power stroke and myofilament sliding in sarcomeres. Synchronized $Ca^{2+}$ release causes whole cell contraction and is readily observable with current microscopy techniques. However, it is unknown whether localized $Ca^{2+}$ release, such as $Ca^{2+}$ sparks and waves, can cause local sarcomere contraction. Contemporary imaging methods fall short of measuring microdomain $Ca^{2+}$-contraction coupling in live cardiac myocytes.**

***Objective:*** **To develop a method for imaging sarcomere level $Ca^{2+}$-contraction coupling in healthy and disease model cardiac myocytes.**

***Methods and Results:*** **Freshly isolated cardiac myocytes were loaded with the $Ca^{2+}$-indicator fluo-4. A confocal microscope equipped with a femtosecond-pulsed near-infrared laser was used to simultaneously excite second harmonic generation from A-bands of myofibrils and 2-photon fluorescence from fluo-4. $Ca^{2+}$ signals and sarcomere strain correlated in space and time with short delays. Furthermore, $Ca^{2+}$ sparks and waves caused contractions in subcellular microdomains, revealing a previously underappreciated role for these events in generating subcellular strain during diastole. $Ca^{2+}$ activity and sarcomere strain were also imaged in paced cardiac myocytes under mechanical load, revealing spontaneous $Ca^{2+}$ waves and correlated local contraction in pressure-overload–induced cardiomyopathy.**

***Conclusions:*** **Multimodal second harmonic generation 2-photon fluorescence microscopy enables the simultaneous observation of $Ca^{2+}$ release and mechanical strain at the subsarcomere level in living cardiac myocytes. The method benefits from the label-free nature of second harmonic generation, which allows A-bands to be imaged independently of T-tubule morphology and simultaneously with $Ca^{2+}$ indicators. Second harmonic generation 2-photon fluorescence imaging is widely applicable to the study of $Ca^{2+}$-contraction coupling and mechanochemotransduction in both health and disease. (*Circ Res*. 2016;118:e19-e28. DOI: 10.1161/CIRCRESAHA.115.307919.)**

**Key Words:** calcium signaling ■ cardiomyopathies ■ mechanotransduction, cellular ■ microscopy, fluorescence, multiphoton ■ multimodal imaging ■ myocardial contraction ■ sarcomeres



Excitation–contraction coupling in cardiac myocytes is mediated by $Ca^{2+}$. During systole, an action potential opens voltage-gated $Ca^{2+}$ channels in the sarcolemma to allow $Ca^{2+}$ entry into the cell, which triggers a much larger release of $Ca^{2+}$ from the sarcoplasmic reticulum through the ryanodine receptor (RyR); this process is termed $Ca^{2+}$-induced $Ca^{2+}$ release. Synchronous $Ca^{2+}$-induced $Ca^{2+}$ release throughout the cell increases the cytosolic $Ca^{2+}$ concentration, and subsequent $Ca^{2+}$ binding to troponin C causes conformational changes in contractile machinery that results in the cross-bridge power stroke and sarcomere contraction. During diastole, cytosolic $Ca^{2+}$ is lowered to basal level by sequestration into the sarcoplasmic reticulum $Ca^{2+}$ store and extrusion from the cell, resulting in sarcomere relaxation.[1]

The RyR cluster is the basic $Ca^{2+}$ release unit in cardiac myocytes. RyR responds to local rises in $Ca^{2+}$ and opens in a stochastic manner. It opens and closes in an all-or-none fashion to release a quantum amount of $Ca^{2+}$, giving rise to

Original received November 6, 2015; revision received December 2, 2015; accepted December 7, 2015. In November 2015, the average time from submission to first decision for all original research papers submitted to *Circulation Research* was 15.52 days.

From the Center for Biophotonics (S.A., Z.M., A.L., D.L.M., J.W.C.), Division of Cardiology (D.K.L., N.C., Y.C.-I.), Division of Hematology/Oncology, Department of Internal Medicine (K.S.L.), and Department of Pathology and Laboratory Medicine (J.W.C.), UC Davis School of Medicine, University of California, Davis, Sacramento; and Departments of Pharmacology (L.T.I., Z.J., T.L., J.B., B.W., Y.-J.C., Y.C.-I.), Biomedical Engineering (S.A., R.S., R.W., Y.C.-I.), Biochemistry and Molecular Medicine (K.S.L.), and Microsurgery Core (Y.-J.C.), University of California, Davis.

*These authors contributed equally to this article.

**The online-only Data Supplement is available with this article at http://circres.ahajournals.org/lookup/suppl/doi:10.1161/CIRCRESAHA.115.307919/-/DC1.**

Correspondence to James W. Chan, Department of Pathology and Laboratory Medicine, University of California, Davis, 2700 Stockton Blvd, Suite 1400, Sacramento, CA 95817. E-mail jwjchan@ucdavis.edu; or Ye Chen-Izu, Departments of Pharmacology, Bioengineering, Internal Medicine/Cardiology, University of California, Davis, 451 Health Science Dr, Tupper Hall 2221, Davis, CA 95616. E-mail ychenizu@ucdavis.edu

| Nonstandard Abbreviations and Acronyms | |
|---|---|
| 2PF | 2-photon fluorescence |
| FFT | fast Fourier transform |
| RyR | ryanodine receptor |
| SHG | second harmonic generation |

a $Ca^{2+}$ spark. The distribution of $Ca^{2+}$ release units in cardiac myocytes shows a lattice-like registered pattern in alignment with sarcomere structure.[2,3] Synchronous opening of $Ca^{2+}$ release units throughout the cell causes a uniform $Ca^{2+}$ transient and coordinated whole-cell contraction. Asynchronous opening of RyRs, however, causes nonuniform rises of $Ca^{2+}$ in local microdomains, manifesting as $Ca^{2+}$ sparks and waves.[4–6] Although healthy cardiac myocytes are largely quiescent and relaxed at rest, studies have shown that various pathological conditions can increase the occurrence of $Ca^{2+}$ sparks and waves during diastole in cardiac myocytes.[7–11]

It is plausible that $Ca^{2+}$ sparks and waves cause $Ca^{2+}$ binding to troponin C and myofilament contraction in local sarcomeres, potentially increasing mechanical strain and stress within the cardiac myocyte. Mechanical stress is linked to cardiac dysfunction and arrhythmias in conditions such as hypertension, myocardial infarction, atrial fibrillation and ventricular tachycardia/fibrillation.[12] Such links are well established at the whole heart level in clinical medicine, but the underlying cellular and molecular mechanisms remain unclear. We speculate that local nonuniform contraction may contribute to disease development via mechanochemotransduction pathways and by affecting cardiac myocyte contractility. Therefore, it is important to investigate local $Ca^{2+}$ release and the mechanical response at the sarcomere level, constituting the basic unit of contraction.

Previously, several techniques have been used to measure sarcomere shortening during cardiac myocyte contraction, including cell-edge detection, sarcomere pattern analysis (using fast Fourier transform [FFT] or autocorrelation-based algorithms), T-tubule labeling with ANEP dyes[13] and quantum dots,[14] and sarcomere structure labeling using genetic expression of fluorescent proteins.[15] However, each of those methods falls short of providing a practical and reliable method for measuring sarcomere contraction in subcellular microdomains. The video-based edge detection method measures cell contraction as the sum of all sarcomere contractions; local contraction cannot be isolated. Sarcomere pattern analysis measures an averaged sarcomere length from the FFT of many sarcomeres. T-tubule labeling methods cannot be applied to disease models in which the T-tubule distribution is irregular or detubulated, such as in heart failure.[16,17] Genetic labeling of the sarcomere with fluorescent proteins is labor-intensive, and some studies suggest that green fluorescent protein (GFP) directly affects cardiac myocyte contractility.[18–20] Moreover, genetic labeling needs to be executed and validated in each new disease model, which is nontrivial. The GFP spectrum also overlaps with the emission spectrum of commonly used $Ca^{2+}$ indicators such as fluo-3 and fluo-4 and therefore interferes with high-resolution $Ca^{2+}$-contraction imaging. Despite these drawbacks, these studies and others in skeletal muscle[21] have been able to show nonuniform sarcomere length changes in spatially uniform $Ca^{2+}$ concentrations.

In this project, we develop an easy-to-use and widely applicable multimodal imaging technique to simultaneously image $Ca^{2+}$ levels and sarcomere contraction at high spatial and temporal resolutions. We image sarcomere contraction in a label-free manner by using second harmonic generation (SHG) to track A-bands in subsarcomere structure in live cardiac myocytes. We further integrate SHG with 2-photon fluorescence (2PF) microscopy to measure $Ca^{2+}$ release. Importantly, the multimodal technique is superbly suited for imaging live cells in real time because SHG microscopy does not require the use of an exogenous label or genetic modification. Furthermore, a single laser can be used to excite SHG and 2PF, providing inherent spatial and temporal colocalization of the signals.

In what follows, we demonstrate how to use the technique to simultaneously image local $Ca^{2+}$ signals and sarcomere contraction, and we also present the computational methods for data analysis. These provide a complete toolbox for using SHG-2PF microscopy to investigate various cell models. We then use the multimodal technique to reveal that localized $Ca^{2+}$ release events can cause local sarcomere contractions in subcellular microdomains in both healthy and diseased cells. Specifically, a $Ca^{2+}$ spark can cause sarcomere contraction (termed myo-pinch), and a $Ca^{2+}$ wave can cause sequential contraction of adjacent sarcomeres. We also apply the SHG-2PF method to image aberrant $Ca^{2+}$ and contractions in paced cardiac myocytes under mechanical load. The data reveal a phenomenon of spontaneous $Ca^{2+}$ waves and local contraction occurring between paced transients in pressure-overload–induced cardiomyopathy. Our observations, enabled by SHG-2PF imaging, raise the possibility that $Ca^{2+}$ sparks and waves increase internal mechanical strain and stress in cardiac myocytes and may therefore contribute to alterations in cellular mechanochemotransduction signaling.

## Methods

All laboratory procedures in this study conform to the Guide for the Care and Use of Laboratory Animals published by the US National Institutes of Health, the Guide for the Care and Use of Laboratory Animals laid out by Animal Care Committee of the University of California. The animal use was approved by the University of California Davis Institutional Animal Care and Use Committee. Cell isolation, dye loading, and antibody labeling protocols are available in the Online Data Supplement.

### SHG-2PF Imaging

SHG is a process in which light of wavelength λ produces its second harmonic (wavelength ½ λ) as it passes through a noncentrosymmetric medium. The process is coherent, so the medium must have a long-range order and orientation that allows constructive interference of the second harmonic signal. SHG was first demonstrated in noncentrosymmetric crystals,[22] but has since been demonstrated in biological macromolecules, including collagen, tubulin arrays, and sarcomeric myosin.[23–27] SHG occurs strongly when these macromolecules are highly ordered, as they are in tendons, axons, and striated muscle. Because the properties that enable SHG are intrinsic to the macromolecules themselves, exciting and detecting SHG in muscle does not require the use of exogenous or genetic labels; furthermore, SHG is a nonabsorptive process, and thus is not prone to photobleaching. Several groups have studied SHG in sarcomeric myosin in depth—together, they have shown both the myosin rod and head domains of the

thick filaments contribute to the generated signal, whereas the actin thin filaments do not.[26,28,29] The label-free nature of sarcomeric SHG has been used to study sarcomere microarchitecture in muscular dystrophy,[30,31] myofibrilogenesis,[32] and drug-induced myopathy.[33] It has also been developed as a technique to study local actin-myosin cross-bridging[28,29] and in vivo contractile dynamics in skeletal muscle.[34] Boulesteix et al[35] have used it to measure sarcomere length with a reported accuracy of 20 nm in relaxed and tetanic frog cardiac myocytes.

SHG can be readily integrated with 2PF microscopy. In 2PF, laser light of wavelength $\lambda_{ex}$ is used to excite an electron transition at energy $½\,\lambda_{ex}$. After the loss of vibrational energy, a Stokes-shifted photon is emitted at $\lambda_{em}>½\,\lambda_{ex}$. The shift allows the signal from fluorophores ($\lambda_{em}>½\,\lambda_{ex}$) and harmonophores ($\lambda_{em}=½\,\lambda_{ex}$) to be simultaneously excited, separated, and detected (Figure 1).

For our experiments, a Coherent Chameleon outputting 150 fs pulses at a repetition rate of 80 MHz and tuned to a wavelength of 976 nm was used as the excitation source; laser power at the sample was typically 12 mW. The laser was air-coupled to an Olympus FluoView 300 (FV300) scanning unit with an IX-81 microscope. A 60×/1.2 N.A. water immersion objective was used as the excitation objective. Two-photon excitation at half of the 976-nm wavelength was used to excite $Ca^{2+}$ indicator fluo-4.

2PF was collected in the epi-direction, separated from the excitation beam with a dichroic mirror, and isolated with a 550±40-nm bandpass filter. SHG was collected in the forward direction with a 50×/0.55 NA extra-long working distance objective and isolated with a 488±10-nm bandpass filter. Emission from SHG and 2PF was simultaneously collected through 2 separate photon multiplier tubes. The spatial and temporal resolutions of the SHG-2PF images are defined by the confocal microscope with maximal of $x,y$=0.25 µm, $z$=0.8 µm, $t$=3 µs/pixel. Two-dimensional (2D) raster and 1D line scan images were acquired using the Olympus FluoView software. Postprocessing and data analysis were performed using Fiji and Matlab software and are described below.

## Results

### Localization of SHG to Known Contractile and $Ca^{2+}$-Handling Structures

Previous work has shown that SHG signals from cardiac myocytes originate from the myosin heads of the thick filament and

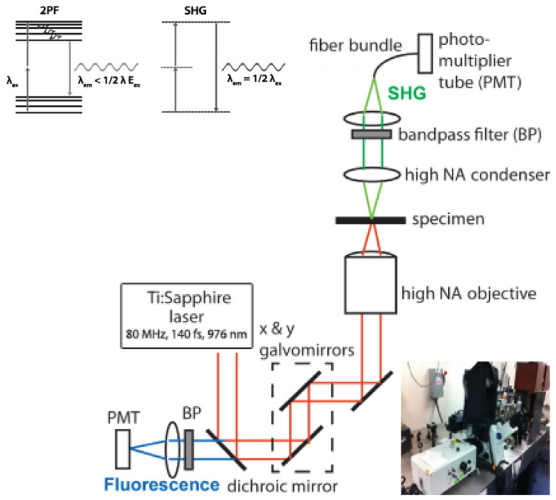


**Figure 1. Basics of multimodal second harmonic generation-2-photon fluorescence (SHG-2PF) imaging.** Jablonski diagrams help distinguish SHG and 2PF. Two photons excite a transition between states in both processes; the states are virtual in SHG and real in 2PF. Vibration reduces the energy of the excited state before 2PF emission. In contrast, no relaxation occurs with SHG. The schematic of our setup, detailed in the text, is depicted above. BP indicates bandpass filter; and NA, numerical aperture.

therefore show the position of the A-bands in sarcomere.[25,26] On the basis of known ultrastructure, we illustrated the localization of SHG signals in relation to the major structures governing $Ca^{2+}$-triggered contraction in the sarcomere in Figure 2A. We used SHG-2PF imaging to experimentally verify the localization of SHG signals as discussed. In 1 set of experiments, we immunolabeled RyRs using antibodies conjugated with Alexa Fluor 488 (AF-488) and subsequently performed multimodal SHG-2PF microscopy as described above. Figure 2B shows the dual SHG-2PF image so obtained, with punctate RyR staining appearing in sets of A-bands. An enlarged view of a single sarcomere shows that the A-bands and RyR clusters in the SHG-2PF image indeed correspond to the known ultrastructure of cardiac myocytes.

To visualize the localization of SHG signal with respect to the T-tubules, we used Di8-ANEPPS (Di8) to label sarcolemma and T-tubules in live cardiac myocytes. Using a 2D fast scan, we visualized the entire cardiac myocyte and identified a single myofilament to interrogate further. We then used the confocal linescan mode to obtain fast 1-dimensional SHG-2PF linescans of the myofilament, which are required to capture fast dynamics in live cardiac myocytes. Figure 2C shows the linescan image acquired by scanning along a single myofilament repetitively. The SHG signal (green) shows the A-bands, whereas the 2PF signal (purple) shows the Di8-labeled T-tubules. In accordance with known ultrastructure and previous microscopy studies, 2 A-bands are seen within each sarcomere, flanked by a pair of T-tubules. The fluorescence intensity profiles (bottom panel) allow the quantifying of the position and distance between these SHG-2PF signals.

### Simultaneous Imaging of the A-Band and $Ca^{2+}$ at High Spatial and Temporal Resolution

To image $Ca^{2+}$-contraction coupling, we loaded freshly isolated cardiac myocytes with the fluorescent $Ca^{2+}$ indicator fluo-4. Figure 3 shows a sample SHG-2PF linescan image acquired at a spatial resolution of 1024 pixels per line, and a temporal resolution of 9.3 ms per line (9.1 µs/pixel). A $Ca^{2+}$ transient is seen in the increase of fluo-4 fluorescence (Figure 3A, left), and the triggered sarcomere contraction is seen from the displacement of the SHG signals (Figure 3A, right). Subsequent linescans were obtained at faster speeds of 3.1 ms per line (≈3.1 µs/pixel).

To resolve sarcomere contraction from the SHG signals, we calculated the distance between adjacent A-bands. As illustrated in Figure 3B, we denote $L_M$ as the distance between the 2 A-bands within the same sarcomere (seen between the T-tubules, traversing the M-line), and $L_Z$ as the distance between the adjacent A-bands across the sarcomere (seen across the T-tubule, traversing the Z-line). $L_M$ and $L_Z$ each can be measured from the distance between the adjacent SHG-bright bands. During contraction, $L_Z$ is shortened by increased overlap of the thick and thin filaments, whereas the $L_M$ remains unchanged because the length of the thick filament within a sarcomere does not change. The sum of $L_M$ and $L_Z$ is equal to the sarcomere length, $L_{SL}=L_M+L_Z$ (eg, the distance from Z-line to Z-line, or equivalently from M-line to M-line).

We used the above definitions to measure $L_M$ and $L_Z$ from the distance between the SHG-bright bands in Figure 3C. The

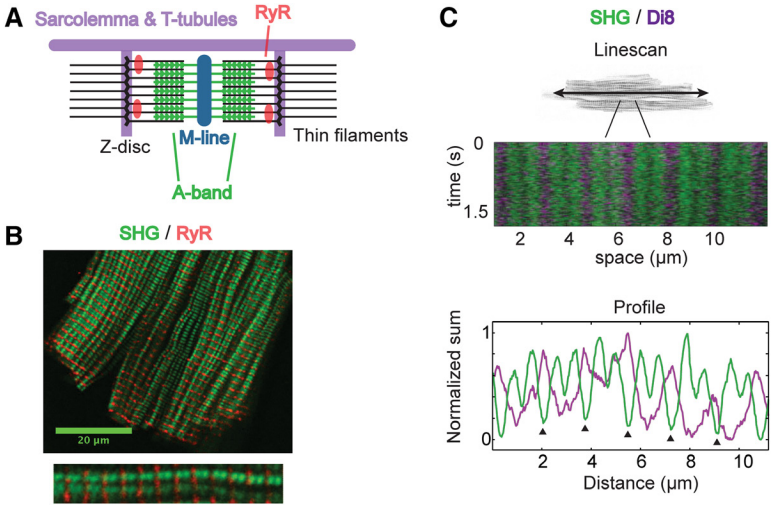


**Figure 2. Second harmonic generation (SHG) localizes to the thick filaments of sarcomeres.** SHG originates from the thick filaments of sarcomeres. Ryanodine receptors (RyRs) reside on the sarcoplasmic reticulum, adjacent to Z discs. T-tubules course along myofilaments and wrap around Z discs. **A**, The localization of these structures to sarcomeric SHG. **B**, SHG (green)-2-photon fluorescence (red) imaging of a rat ventricular cardiomyocyte immunostained using anti–RYR2-AF488 antibodies, with a single myofilament enlarged below. **C**, A multimodal line scan along a single myofilament in a live rVCM loaded with Di8-ANEPPS. Below is a plot of the signals summed in time, showing the double-banding pattern of sarcomeric SHG with deeper minima (arrowheads) corresponding Z-disc locations.



histogram of inter-A-band distances can be calculated using the kernel density method (Online Methods).[36,37] During diastole (Figure 3A, green framed region), the histogram of distances between adjacent A-bands shows 2 distinct peaks (Figure 3C, green curves), corresponding to $L_M$=0.8 µm and $L_Z$=1.0 µm. During systole (Figure 3A, red framed region), the histogram also shows 2 peaks (Figure 3C, red curves), but corresponding to $L_M$=0.8 µm and $L_Z$=0.9 µm. Thus, in agreement with our analysis, $L_M$ is constant and $L_Z$ is shortened during contraction. The calculated sarcomere lengths $L_{SL}=L_M+L_Z$ in these states are $L_{SL}$=1.8 µm at diastole (the slack length in an isolated cardiac myocyte) and $L_{SL}$=1.6 µm at systole. To verify the sarcomere length values calculated using the SHG image, we also directly measured the sarcomere length from the transmission image of the myocyte using an established method (Online Figure I). We obtained a sarcomere length of 1.8 µm at diastole and 1.6 µm at systole, in agreement with the values calculated from the SHG image.

## Construction of Strain Maps of Sarcomere Contraction From SHG Image Analysis

We developed an automated image analysis method to extract local sarcomere contraction information from the SHG linescan images. Figure 4 depicts the analysis procedure. First, we reduced the noise in the raw SHG image data by applying a 2D Wiener filter (Figure 4B). The Wiener filter requires the neighborhood size of the relevant image features to be defined. In the SHG linescan image, the neighborhood in space is set to roughly one half of the width of the more narrow SHG dark bands (which corresponds to the M-line positions). The neighborhood in time is set according to the speed and magnitude of contractions that are present in the data (eg, if the contractions are rapid and involve significant translation, a small time neighborhood is chosen). Second, after noise reduction, a 2D FFT of the spatial SHG signal is performed line-by-line, and then each FFT is bandpass filtered (Figure 4C). The band that is retained corresponds to spatial periods of 300 nm to 2.5 µm and contains the key spatial frequencies and phases of the A-band signal. Each line is then inverse Fourier transformed to obtain a smooth, oscillating signal that is in phase with the SHG-bright bands (Figure 4D). Third, from this signal, the minima between SHG-bright bands are obtained (Figure 4E, red lines), which are used to set processing windows around the SHG-bright bands. Gaussian fitting is then used to estimate the center of each SHG-bright band at each point in time. The results of Gaussian fitting (Figure 4F, yellow lines), therefore, estimate the center of the A-bands. The distance between the center of the A-bands corresponds to the $L_M$ and $L_Z$ peaks as discussed previously. Histograms of the center-to-center distances during diastole and systole show that myocyte contraction shortens $L_Z$, whereas $L_M$ remains unchanged (Figure

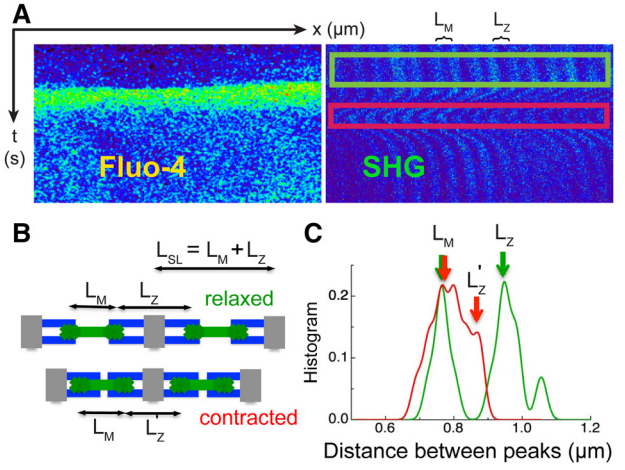


**Figure 3. Relationship between sarcomere structure and A-band position. A**, Second harmonic generation-2-photon fluorescence (SHG-2PF) linescan imaging of the myocyte shows a $Ca^{2+}$ transient seen in the fluo-4 signal (**top left** of images on right) and the triggered contraction in the SHG signal (**top right**). **B**, $L_M$ is the distance between 2 adjacent A-bands within the same sarcomere. $L_Z$ is the distance between the 2 A-bands across the adjacent sarcomeres. The sarcomere length $L_{SL}$ is equal to the sum of $L_M$ and $L_Z$. $L_Z$ shortens during cell contraction because of the sliding of the thick filament against the thin filament. **C**, The histogram of A-bands distances is calculated using the kernel density method described in the online Methods. $L_M$ is determined by the thick filament structure within the sarcomere and does not change during cell contraction. $L_Z$ shortens as described. The numerical values of $L_{SL}$ during systole and diastole calculated in this way match with sarcomere length calculated using a Fourier transform–based method in a similar myocyte (Online Figure I).

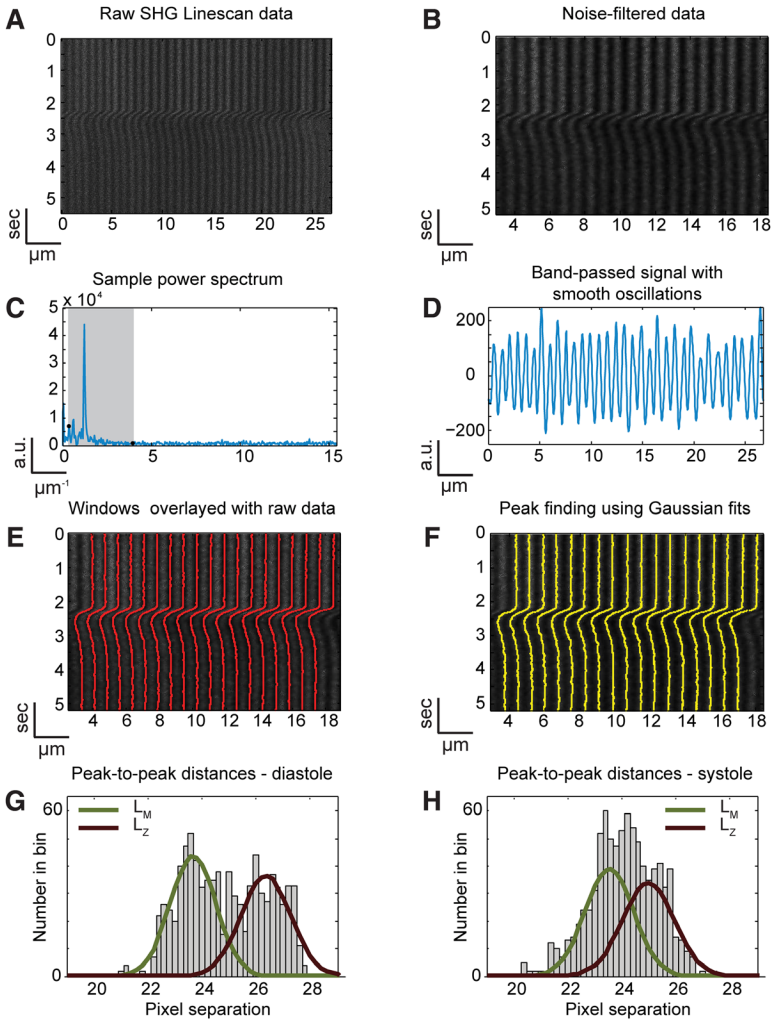


**Figure 4. Centers of second harmonic generation (SHG)-bright bands can be identified at each time point**. To track the peaks of the SHG bands in the raw data (**A**), noise-filtered data (**B**) is Fourier transformed and bandpass filtered (**C**) to obtain a smoothly varying signal (**D**) from which windows for peak fitting can be readily defined (**E**). Next, each SHG band is fit with a Gaussian at each point in time to determine the center of each SHG band (**F**). These centers are then used for further analysis. Histograms of the center-to-center distances during diastole (**G**, corresponding to time frame indicated by the **top** most black bar to the right of **F**) and systole (**H**, **bottom** black bar of **F**) show that $L_M$ does not change during contraction, whereas $L_Z$ shortens, as expected from Figure 3. The displayed Gaussian fits of the histogram data come from fitting single Gaussian functions to the $L_M$ and $L_Z$ data separately (Online Figure II).

4G and 4H; Online Figure II). Thus, our automated analysis is able to extract expected changes in the distances between adjacent A-bands.

Next, we construct a strain map that displays sarcomere contraction and relaxation through time by using the centers of the SHG-bright bands. We first use a moving local linear regression to smooth the data through time (Online Figures III and IV). The strain over a given sarcomeric distance is then calculated as $E=(L_o-L)/L_0$, where $L$ is the distance between a SHG-bright band and its next nearest neighbor, and $L_0$ is that distance averaged over the first 25 pixels in time (when the cell is relaxed). Figure 5 (middle panels) shows sample strain maps computed from the SHG-2PF images obtained from cardiac myocytes at different contractile states.

## Correlation Between $Ca^{2+}$ and Strain Maps in Cardiac Myocytes at Different Contractile States

To investigate local $Ca^{2+}$-contraction coupling, we plotted the strain map and $Ca^{2+}$ image side-by-side in Figure 5. Figure 5A shows a relaxed state with no development of strain (left and middle panels) at low resting $Ca^{2+}$ concentration (right panel). Figure 5B shows a development of strain across sarcomeres (left and middle panels) in response to a propagating $Ca^{2+}$ wave (right panel). Higher strain correlates to higher $Ca^{2+}$ in space, and a time lag between $Ca^{2+}$ rise and strain development can be observed. Figure 6A demonstrates that the normalized cross-correlation between the strain and the corresponding $Ca^{2+}$ signal ranges from 0.90 to 0.93 for the sarcomere lanes seen in Figure 5B (mean=0.92; σ=0.01); the time delay to the cross-correlation maximum ranges from 114.7 to 192.2 ms (mean=149.3 ms; σ=30.3 ms). These delays are in agreement with the observation at the whole-cell level that there is a lag between the $Ca^{2+}$ transient and the cardiac myocyte contraction.[38] Thus, multimodal SHG-2PF microscopy is capable of capturing the sequential development of strain in individual sarcomeres in response to a propagating $Ca^{2+}$ wave.

The method also enables us to answer a previously unresolved question: Do $Ca^{2+}$ sparks cause local sarcomere contraction? To analyze the correlation between $Ca^{2+}$ sparks and the nearest neighbor A-bands, we computed the strain map from M-line to M-line (Figure 5C, middle panel). Figure 5C shows the development of microdomain strain (middle panel) in response to localized $Ca^{2+}$ sparks (right panel). A positive correlation between $Ca^{2+}$ sparks and local strain can be observed although the time delay for strain development is variable (addressed below). Thus, $Ca^{2+}$ sparks can indeed cause local sarcomere contractions (myo-pinch) that lead to nonuniform strain in subcellular microdomains.

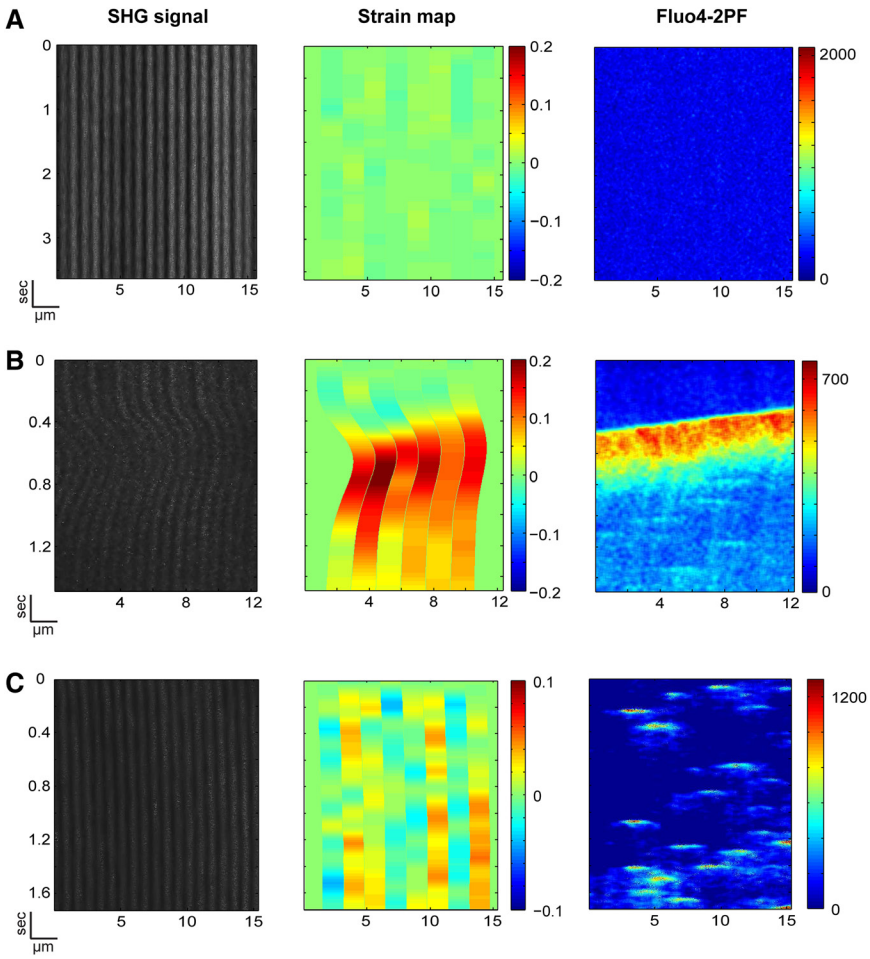


**Figure 5. Strain maps constructed from second harmonic generation (SHG)-bright bands demonstrate local calcium-correlated contraction.** Strain across a sarcomere length is calculated using the distance between every other SHG-bright band, $L$, and the average of that distance for the first 25 pixels in time, $L_0$. Strain is $(L–L_0)/L_0$. **A–C**, **Left**, The noise-filtered raw data. **Right**, Simultaneously obtained 2-photon fluorescence (2PF) signals from fluo-4-AM. **A**, A negative control—a rat VCM at resting state. **B**, A contraction in which transient nonuniform strain develops in response to a calcium wave. **C**, A strain map, interpolated onto an M-line to M-line grid, resulting from calcium sparks. The area of zero strain on either side of each strain map is an edge artifact; strain was not calculated in these regions.

In Figure 6C, events from Figure 5C with an apparent spark strain correlation (Figure 6B) are plotted separately. In these plots, history dependence can be observed: peak strain develops earlier for sparks that occur shortly after a previous spark-strain event (Figure 6C, plots 1, 2, 4, and 5: average time to peak strain=176.2 ms) than for those with a longer strain-free history (Figure 6C, plots 3, 7, and 8: average time to peak strain=75.4 ms). Some of the $Ca^{2+}$ spark–induced myo-pinches are small in magnitude; we excluded those that are outside of our 85% confidence intervals on strain (Online Figure V). In addition, we examined the effect of our smoothing algorithm on $Ca^{2+}$ spark–induced myo-pinch and on simulated strain and confirmed that smoothing does not attenuate strain events that lasts for ≥60 ms (Online Figures VI and VII); myo-pinch events lasted >100 ms in our observations.

### $Ca^{2+}$-Contraction Coupling in a Murine Model of Pressure-Overload–Induced Cardiomyopathy

To demonstrate the utility of the SHG-2PF imaging modality in disease model animals, we used transverse aortic constriction surgery to generate pressure-overload mice that develop cardiac hypertrophy and heart failure[39] (online Methods). Cardiac myocytes from transverse aortic constriction mice were studied under mechanical load using the cell-in-gel system as previously described,[40] as well as under standard load-free conditions. When load-free, transverse aortic constriction cardiac myocytes responded to electrical pacing with regular contractions (Figure 7A). Under mechanical load, however, the cells displayed aberrant spontaneous $Ca^{2+}$ waves at variable times during diastole, between paced systolic $Ca^{2+}$ transients (Figure 7B). Figure 7C to 7E shows a strain map analysis of one such aberrant $Ca^{2+}$ wave, among paced transients, in a transverse aortic constriction cardiac myocyte under mechanical load. Figure 7C shows the SHG data, D shows the strain map obtained from an analysis of 2 adjacent sarcomeres, and E shows the corresponding 2PF data. At the single sarcomere level (Figure 7F and 7G), the wave-triggered contractions were lower in amplitude than in the paced contractions. Consistently, the amplitude of the contractions correlated to the relative change in intrasarcomere calcium levels. These results demonstrate the applicability of the SHG-2PF technique to study of mechanical stress–induced heart disease.

## Discussion

Imaging local $Ca^{2+}$-contraction coupling at sarcomere resolution in cardiac myocytes is difficult with available techniques yet necessary for investigating the molecular mechanisms that link mechanical stress to heart diseases. In this project, we developed a multimodal SHG-2PF technique to image $Ca^{2+}$-induced strain at the single sarcomere level. The technique used a single laser to excite SHG from the thick filaments of sarcomeres and 2PF from a fluorescent $Ca^{2+}$ indicator, simultaneously. First, we developed the methods and algorithms for acquiring, processing, and interpreting the multimodal

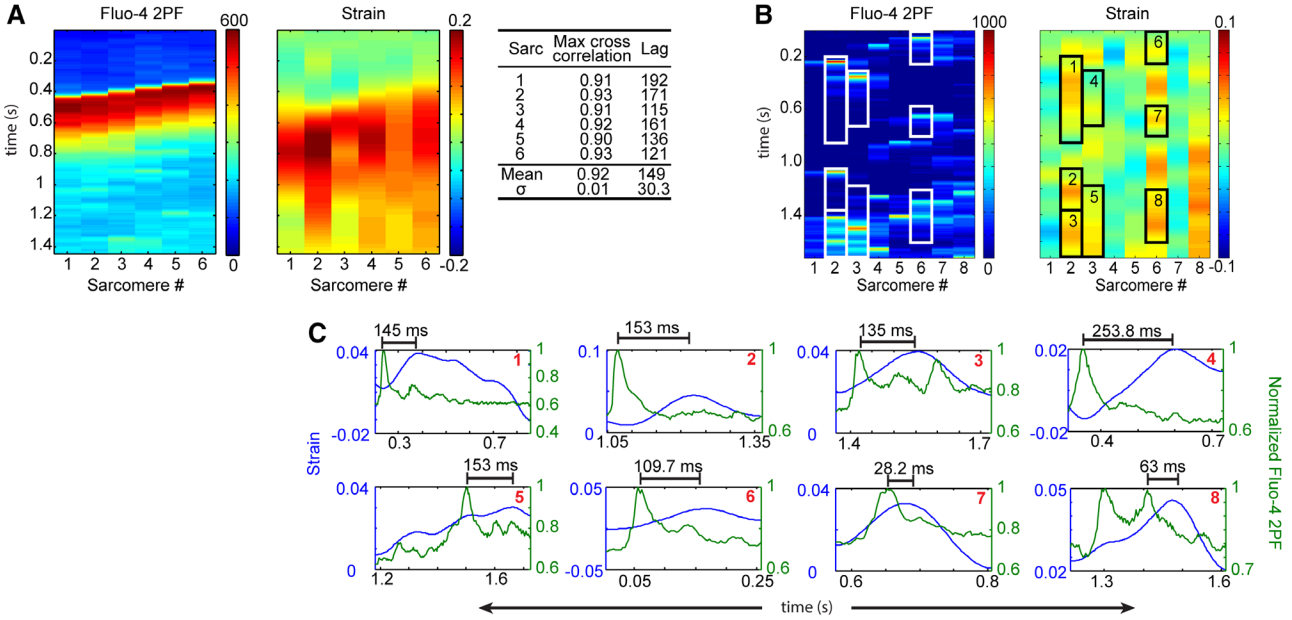


| Sarc | Max cross correlation | Lag |
|---|---|---|
| 1 | 0.91 | 192 |
| 2 | 0.93 | 171 |
| 3 | 0.91 | 115 |
| 4 | 0.92 | 161 |
| 5 | 0.90 | 136 |
| 6 | 0.93 | 121 |
| Mean | 0.92 | 149 |
| σ | 0.01 | 30.3 |

**Figure 6. Deeper analysis of sarcomere-scale calcium-contraction coupling**. **A**, Average fluo-4 2-photon fluorescence (2PF) across distances over which strain was calculated, for a calcium wave, next to strain. Table, The normalized cross-correlations between 2PF and strain for each lane. **B**, Average fluo-4-2PF across distances over which strain was calculated, next to strain, during calcium sparks. Myo-pinch phenomena that lie within 85% confidence intervals are boxed and plotted individually in **C**.

image data. Second, we verified the SHG analysis by comparing the SHG signal to the known ultrastructure of sarcomere and the $Ca^{2+}$-handling molecules (ie, A-band, T-tubule, and RyRs). Third, we tested the feasibility of using the SHG-2PF technique to simultaneously image $Ca^{2+}$ and sarcomere contractions. We were able to make the novel observation in live cardiac myocytes that $Ca^{2+}$ sparks can induce local mechanical strain at the sarcomere level, a phenomenon we named myo-pinch. Finally, we applied the technique to a murine model of mechanical stress–induced heart disease; when these cardiac myocytes were placed under mechanical load, we observed calcium waves and associated sarcomere strain occurring between paced transients.

Multimodal SHG-2PF imaging has distinct advantages over other available techniques. Recently, Shintani et al[15] developed a method for measuring sarcomere shortening by labeling the Z-discs with AcGFP-tagged α-actinin for imaging. However, the method uses vector-mediated transfection of cardiac myocytes that requires culturing the cells to express adequate amount of AcGFP-tagged α-actinin. In culture, both neonatal and adult cardiac myocytes undergo changes in the $Ca^{2+}$ handling and contractile characteristics[41–43] and hence may introduce artifacts. Genetic labeling methods are also disadvantaged by potential interference between GFP and sarcomeric protein function.[18] In contrast, we use SHG to accomplish label-free and noninvasive imaging of A-bands within the sarcomeres of live cardiac myocytes.

Another sarcomere-tracking technique uses labeled T-tubules. However, T-tubules in cardiac myocytes, even those from the healthy hearts, display a significant variance in the regularity, direction, diameter, and distance from Z discs.[44] In some disease states such as hypertrophy and heart failure, T-tubule networks can become irregular and detubulated.[45,46] In comparison, SHG is intrinsic to the thick filaments of sarcomere and is detectable as long as the sarcomeres remain intact. Therefore, SHG microscopy is ideally suited for studying sarcomere-level contraction in heart disease models.

Both genetic labeling and T-tubule labeling are further restrictive when used in conjunction with fluorescent $Ca^{2+}$ indicators for dual imaging. The fluorophores must be carefully selected for each imaging modality in accordance with the kinetics of the indicator and to allow spectral separation. It may not be possible to minimize the cross talk between sarcomere markers such as GFP and fluorescent $Ca^{2+}$ indicators such as fluo-4. The use of SHG circumvents this difficulty because SHG has a signal wavelength of $\lambda_{ex}/2$; any fluorescent label used for 2PF will be Stokes-shifted and separable from the second harmonic signal. Therefore, SHG provides a superb add-on modality for simultaneously imaging sarcomere contraction with $Ca^{2+}$ signals.

The multimodal method as presented enabled us to show that $Ca^{2+}$ sparks can cause local sarcomere contractions. However, it can be further refined to increase the signal:noise (S/N) ratio and improve the quantification of small contraction events. One way to address this is to raise the laser power. In our preliminary experiments, however, higher laser powers than what were used caused some degree of laser-induced $Ca^{2+}$ release and photon damage and therefore limited the achievable S/N ratio for SHG. For future improvements, several approaches can increase the S/N ratio in multiphoton microscopes. For example, our original equipment manufacturer-installed fiber bundle that collects forward-directed light does not collect 100% of the photons; bypassing the fiber and collecting SHG photons directly using a photon multiplier tube would double the SHG signal.[47,48] Compressing the femtosecond laser pulses used to excite SHG and 2PF by chirping can significantly improve S/N ratio in multiphoton processes because generated signals scale quadratically with the peak power of the pulse.[49] These approaches can

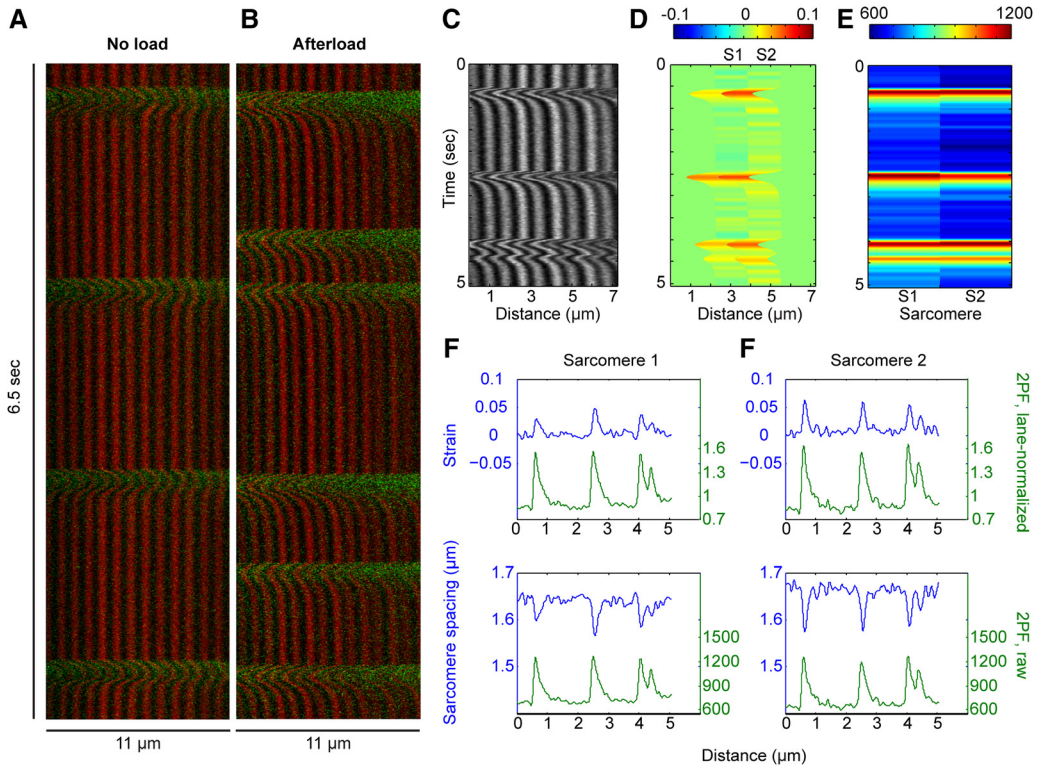


**Figure 7. Multimodal second harmonic generation-2-photon fluorescence (SHG-2PF) imaging of cardiac myocytes from transverse aortic constriction (TAC) mice**. **A**, SHG (red) and 2PF (green) data from an isolated TAC cardiac myocyte under no load, paced at 0.5 Hz. **B**, SHG and 2PF data from a TAC cardiac myocyte embedded in a gel to produce afterload, showing calcium tides while being paced at 0.5 Hz. **C** and **D**, Strain map analysis of a localized 2-sarcomere region from a TAC cardiac myocyte under afterload and 0.5 Hz pacing. **E**, 2PF signal within the corresponding sarcomeres from **D**. **F** and **G**, Plots of sarcomere strain vs lane-normalized 2PF (**top**) and sarcomere spacing vs raw 2PF (**bottom**).

be combined to improve the S/N ratio and therefore our ability to estimate the center of mass of the A-bands.

A potential limitation of the SHG-2PF method lies in measuring strain during global (eg, electrically stimulated) contractions in load-free cardiac myocytes if the motion is too large to keep the same sarcomere within the focus of the confocal microscope. Because of the highly localized nature of the SHG-2PF technique, it is best used to track local sarcomere contraction in response to local $Ca^{2+}$ releases. For the measurement of global contractions, however, there are many established methods (edge detection, sarcomere pattern measurement using FFT, etc). The main advantage of the technique we developed here is that it allows one to zoom in and measure microdomain contraction—morphological changes in A-bands within individual sarcomeres—in response to local $Ca^{2+}$ signals.

Super resolution microscopy is a rapidly evolving field and may impact SHG-2PF imaging in the future. A-bands are readily resolvable with our current technique, but any improvement in resolution will improve precision in the determination of A-band centers. Although no super resolution method currently exists for harmonic generation microscopy, several investigators are actively developing label-free super resolution methods.[50,51] As a special consideration to $Ca^{2+}$ imaging, the usefulness of super resolution methods is limited by the fact that $Ca^{2+}$ diffuses rapidly, and small-molecule $Ca^{2+}$ indicators also have limited on/off kinetics. A promising approach may be to express localized $Ca^{2+}$ indicators[52–55] in subcellular compartments to further quantify local $Ca^{2+}$ levels in relation to sarcomere strain.

In summary, we have developed multimodal SHG-2PF imaging as a new, enabling tool for simultaneously imaging $Ca^{2+}$ levels and sarcomere contraction in live cardiac myocytes with confocal resolution. Our method permits the investigation of the relationship between localized $Ca^{2+}$ release events and mechanical strain in subcellular microdomains. Such knowledge is important for understanding the mechanochemotransduction within the cell that contributes to mechanical stress–induced heart diseases.

## Acknowledgements

S. Awasthi thank the California Institute of Regenerative Medicine's Stem Cell Training Program at UC Davis and the UC Davis Physician-Scientist Training Program for graduate student scholarships.

## Sources of Funding

This work was supported by a UC Davis Academic Senate Faculty Research grant to J.W. Chan and Y. Chen-Izu, National Institutes of Health (NIH) R01HL90880 and R01HL105242 to L.T. Izu and Y. Chen-Izu, NIH R01HL123526 to Y. Chen-Izu, R03AG031944 to Y. Chen-Izu, R01HL105242 to L.T. Izu. R01HL85844 and HL85727 to N. Chiamvimonvat, National Science Foundation 1264776 to J.W. Chan and D.K. Lieu, and by the Center for Biophotonics, National Science Foundation Science and Technology Center that is managed by the University of California, Davis, under cooperative agreement No. PHY 0120999. This work is also supported, in part, by the University of California startup funds to Y. Chen-Izu.

## Disclosures

None.

## References


1. Bers DM. *Excitation-Contraction Coupling and Cardiac Contractile Force*. 2nd ed. Dordrecht: Kluwer Academic Publishers; 2001.
2. Chen-Izu Y, McCulle SL, Ward CW, Soeller C, Allen BM, Rabang C, Cannell MB, Balke CW, Izu LT. Three-dimensional distribution of ryanodine receptor clusters in cardiac myocytes. *Biophys J*. 2006;91:1–13. doi: 10.1529/biophysj.105.077180.
3. Soeller C, Jayasinghe ID, Li P, Holden AV, Cannell MB. Three-dimensional high-resolution imaging of cardiac proteins to construct models of intracellular Ca2+ signalling in rat ventricular myocytes. *Exp Physiol*. 2009;94:496–508. doi: 10.1113/expphysiol.2008.043976.
4. Cheng H, Lederer WJ, Cannell MB. Calcium sparks: elementary events underlying excitation-contraction coupling in heart muscle. *Science*. 1993;262:740–744.
5. Cannell MB, Cheng H, Lederer WJ. Spatial non-uniformities in [Ca2+] i during excitation-contraction coupling in cardiac myocytes. *Biophys J*. 1994;67:1942–1956. doi: 10.1016/S0006-3495(94)80677-0.
6. López-López JR, Shacklock PS, Balke CW, Wier WG. Local, stochastic release of Ca2+ in voltage-clamped rat heart cells: visualization with confocal microscopy. *J Physiol*. 1994;480(pt 1):21–29.
7. Boyden PA, Pu J, Pinto J, Keurs HE. Ca(2+) transients and Ca(2+) waves in purkinje cells: role in action potential initiation. *Circ Res*. 2000;86:448–455.
8. Schlotthauer K, Bers DM. Sarcoplasmic reticulum Ca(2+) release causes myocyte depolarization. Underlying mechanism and threshold for triggered action potentials. *Circ Res*. 2000;87:774–780.
9. Berlin JR, Cannell MB, Lederer WJ. Cellular origins of the transient inward current in cardiac myocytes. Role of fluctuations and waves of elevated intracellular calcium. *Circ Res*. 1989;65:115–126.
10. Bers DM. Cardiac sarcoplasmic reticulum calcium leak: basis and roles in cardiac dysfunction. *Annu Rev Physiol*. 2014;76:107–127. doi: 10.1146/annurev-physiol-020911-153308.
11. Cheng H, Lederer WJ. Calcium sparks. *Physiol Rev*. 2008;88:1491–1545. doi: 10.1152/physrev.00030.2007.
12. Balligand JL, Feron O, Dessy C. eNOS activation by physical forces: from short-term regulation of contraction to chronic remodeling of cardiovascular tissues. *Physiol Rev*. 2009;89:481–534. doi: 10.1152/physrev.00042.2007.
13. Bub G, Camelliti P, Bollensdorff C, Stuckey DJ, Picton G, Burton RA, Clarke K, Kohl P. Measurement and analysis of sarcomere length in rat cardiomyocytes in situ and in vitro. *Am J Physiol Heart Circ Physiol*. 2010;298:H1616–H1625. doi: 10.1152/ajpheart.00481.2009.
14. Serizawa T, Terui T, Kagemoto T, Mizuno A, Shimozawa T, Kobirumaki F, Ishiwata S, Kurihara S, Fukuda N. Real-time measurement of the length of a single sarcomere in rat ventricular myocytes: a novel analysis with quantum dots. *Am J Physiol Cell Physiol*. 2011;301:C1116–C1127. doi: 10.1152/ajpcell.00161.2011.
15. Shintani SA, Oyama K, Kobirumaki-Shimozawa F, Ohki T, Ishiwata S, Fukuda N. Sarcomere length nanometry in rat neonatal cardiomyocytes expressed with α-actinin-AcGFP in Z discs. *J Gen Physiol*. 2014;143:513–524. doi: 10.1085/jgp.201311118.
16. Louch WE, Bito V, Heinzel FR, Macianskiene R, Vanhaecke J, Flameng W, Mubagwa K, Sipido KR. Reduced synchrony of Ca2+ release with loss of T-tubules-a comparison to Ca2+ release in human failing cardiomyocytes. *Cardiovasc Res*. 2004;62:63–73. doi: 10.1016/j.cardiores.2003.12.031.
17. Lyon AR, MacLeod KT, Zhang Y, Garcia E, Kanda GK, Lab MJ, Korchev YE, Harding SE, Gorelik J. Loss of T-tubules and other changes to surface topography in ventricular myocytes from failing human and rat heart. *Proc Natl Acad Sci U S A*. 2009;106:6854–6859. doi: 10.1073/pnas.0809777106.
18. Agbulut O, Huet A, Niederländer N, Puceat M, Menasché P, Coirault C. Green fluorescent protein impairs actin-myosin interactions by binding to the actin-binding site of myosin. *J Biol Chem*. 2007;282:10465–10471. doi: 10.1074/jbc.M610418200.
19. Sekar RB, Kizana E, Smith RR, Barth AS, Zhang Y, Tung L. Lentiviral vector-mediated expression of GFP or Kir2. 1 alters the electrophysiology of neonatal rat ventricular myocytes without inducing cytotoxicity. *Am J Physiol Heart Circ Physiol*. 2007;21205:2757–2770.
20. Nishimura S, Nagai S, Sata M, Katoh M, Yamashita H, Saeki Y, Nagai R, Sugiura S. Expression of green fluorescent protein impairs the force-generating ability of isolated rat ventricular cardiomyocytes. *Mol Cell Biochem*. 2006;286:59–65. doi: 10.1007/s11010-005-9090-6.
21. Telley IA, Denoth J, Stüssi E, Pfitzer G, Stehle R. Half-sarcomere dynamics in myofibrils during activation and relaxation studied by tracking fluorescent markers. *Biophys J*. 2006;90:514–530. doi: 10.1529/biophysj.105.070334.
22. Franken PA, Hill AE, Peters CW, Weinreich G. Generation of opical harmonics. *Phys Rev Lett*. 1961;7:118–119.
23. Fine S, Hansen WP. Optical second harmonic generation in biological systems. *Appl Opt*. 1971;10:2350–2353.
24. Guo Y, Ho PP, Tirksliunas A, Liu F, Alfano RR. Optical harmonic generation from animal tissues by the use of picosecond and femtosecond laser pulses. *Appl Opt*. 1996;35:6810–6813.
25. Campagnola PJ, Millard AC, Terasaki M, Hoppe PE, Malone CJ, Mohler WA. Three-dimensional high-resolution second-harmonic generation imaging of endogenous structural proteins in biological tissues. *Biophys J*. 2002;82:493–508. doi: 10.1016/S0006-3495(02)75414-3.
26. Plotnikov SV, Millard AC, Campagnola PJ, Mohler WA. Characterization of the myosin-based source for second-harmonic generation from muscle sarcomeres. *Biophys J*. 2006;90:693–703. doi: 10.1529/biophysj.105.071555.
27. Dombeck DA, Kasischke KA, Vishwasrao HD, Ingelsson M, Hyman BT, Webb WW. Uniform polarity microtubule assemblies imaged in native brain tissue by second-harmonic generation microscopy. *Proc Natl Acad Sci U S A*. 2003;100:7081–7086. doi: 10.1073/pnas.0731953100.
28. Nucciotti V, Stringari C, Sacconi L, Vanzi F, Fusi L, Linari M, Piazzesi G, Lombardi V, Pavone FS. Probing myosin structural conformation in vivo by second-harmonic generation microscopy. *Proc Natl Acad Sci U S A*. 2010;107:7763–7768. doi: 10.1073/pnas.0914782107.
29. Schürmann S, von Wegner F, Fink RH, Friedrich O, Vogel M. Second harmonic generation microscopy probes different states of motor protein interaction in myofibrils. *Biophys J*. 2010;99:1842–1851. doi: 10.1016/j.bpj.2010.07.005.
30. Plotnikov SV, Kenny AM, Walsh SJ, Zubrowski B, Joseph C, Scranton VL, Kuchel GA, Dauser D, Xu M, Pilbeam CC, Adams DJ, Dougherty RP, Campagnola PJ, Mohler WA. Measurement of muscle disease by quantitative second-harmonic generation imaging. *J Biomed Opt*. 2008;13:044018. doi: 10.1117/1.2967536.
31. Friedrich O, Both M, Weber C, Schürmann S, Teichmann MD, von Wegner F, Fink RH, Vogel M, Chamberlain JS, Garbe C. Microarchitecture is severely compromised but motor protein function is preserved in dystrophic mdx skeletal muscle. *Biophys J*. 2010;98:606–616. doi: 10.1016/j.bpj.2009.11.005.
32. Liu H, Shao Y, Qin W, Runyan RB, Xu M, Ma Z, Borg TK, Markwald R, Gao BZ. Myosin filament assembly onto myofibrils in live neonatal cardiomyocytes observed by TPEF-SHG microscopy. *Cardiovasc Res*. 2013;97:262–270. doi: 10.1093/cvr/cvs328.
33. Huang SH, Hsiao CD, Lin DS, Chow CY, Chang CJ, Liau I. Imaging of zebrafish in vivo with second-harmonic generation reveals shortened sarcomeres associated with myopathy induced by statin. *PLoS One*. 2011;6:e24764. doi: 10.1371/journal.pone.0024764.
34. Llewellyn ME, Barretto RP, Delp SL, Schnitzer MJ. Minimally invasive high-speed imaging of sarcomere contractile dynamics in mice and humans. *Nature*. 2008;454:784–788. doi: 10.1038/nature07104.
35. Boulesteix T, Beaurepaire E, Sauviat MP, Schanne-Klein MC. Second-harmonic microscopy of unstained living cardiac myocytes: measurements of sarcomere length with 20-nm accuracy. *Opt Lett*. 2004;29:2031–2033.
36. Scott DW, Tapia RA, Thompson JR. Kernel density estimation revisited. *Nonlinear Anal Theory Methods Appl*. 1977;1:339–372.
37. Silverman BW. *Density Estimation for Statistics and Data Analysis*. Boca Raton, FL: Chapman and Hall; 1986.
38. Bers DM. Cardiac excitation-contraction coupling. *Nature*. 2002;415:198–205. doi: 10.1038/415198a.
39. Rockman HA, Ross RS, Harris AN, et al. Segregation of atrial-specific and inducible expression of an atrial natriuretic factor transgene in an in vivo murine model of cardiac hypertrophy. *Proc Natl Acad Sci*. 1991;88:8277–8281.
40. Jian Z, Han H, Zhang T, et al. Mechanochemotransduction during cardiomyocyte contraction is mediated by localized nitric oxide signaling. *Sci Signal*. 2014;7:ra27. doi: 10.1126/scisignal.2005046.
41. Husse B, Wussling M. Developmental changes of calcium transients and contractility during the cultivation of rat neonatal cardiomyocytes. *Mol Cell Biochem*. 1996;163-164:13–21.

42. Kostin S, Hein S, Bauer EP, Schaper J. Spatiotemporal development and distribution of intercellular junctions in adult rat cardiomyocytes in culture. *Circ Res*. 1999;85:154–167.
43. Hersch N, Wolters B, Dreissen G, Springer R, Kirchgeßner N, Merkel R, Hoffmann B. The constant beat: cardiomyocytes adapt their forces by equal contraction upon environmental stiffening. *Biol Open*. 2013;2:351–361. doi: 10.1242/bio.20133830.
44. Soeller C, Cannell MB. Examination of the transverse tubular system in living cardiac rat myocytes by 2-photon microscopy and digital image-processing techniques. *Circ Res*. 1999;84:266–275.
45. Heinzel FR, Bito V, Biesmans L, Wu M, Detre E, von Wegner F, Claus P, Dymarkowski S, Maes F, Bogaert J, Rademakers F, D'hooge J, Sipido K. Remodeling of T-tubules and reduced synchrony of Ca2+ release in myocytes from chronically ischemic myocardium. *Circ Res*. 2008;102:338–346. doi: 10.1161/CIRCRESAHA.107.160085.
46. Dibb KM, Clarke JD, Horn MA, Richards MA, Graham HK, Eisner DA, Trafford AW. Characterization of an extensive transverse tubular network in sheep atrial myocytes and its depletion in heart failure. *Circ Heart Fail*. 2009;2:482–489. doi: 10.1161/CIRCHEARTFAILURE.109.852228.
47. Majewska A, Yiu G, Yuste R. A custom-made two-photon microscope and deconvolution system. *Eur J Physiol*. 2000;441:398–408.
48. Nikolenko V, Nemet B, Yuste R. A two-photon and second-harmonic microscope. *Methods*. 2003;30:3–15.
49. Xi P, Andegeko Y, Pestov D, Lovozoy VV, Dantus M. Two-photon imaging using adaptive phase compensated ultrashort laser pulses. *J Biomed Opt*. 2009;14:014002. doi: 10.1117/1.3059629.
50. Chowdhury S, Izatt J. Structured illumination diffraction phase microscopy for broadband, subdiffraction resolution, quantitative phase imaging. *Opt Lett*. 2014;39:1015–1018.
51. Wang P, Slipchenko MN, Mitchell J, Yang C, Potma EO, Xu X, Cheng JX. Far-field Imaging of Non-fluorescent Species with Subdiffraction Resolution. *Nat Photonics*. 2013;7:449–453. doi: 10.1038/nphoton.2013.97.
52. Kaestner L, Scholz A, Tian Q, Ruppenthal S, Tabellion W, Wiesen K, Katus HA, Müller OJ, Kotlikoff MI, Lipp P. Genetically encoded Ca2+ indicators in cardiac myocytes. *Circ Res*. 2014;114:1623–1639. doi: 10.1161/CIRCRESAHA.114.303475.
53. Shang W, Lu F, Sun T, Xu J, Li LL, Wang Y, Wang G, Chen L, Wang X, Cannell MB, Wang SQ, Cheng H. Imaging Ca2+ nanosparks in heart with a new targeted biosensor. *Circ Res*. 2014;114:412–420. doi: 10.1161/CIRCRESAHA.114.302938.
54. Luo X, Hill JA. $Ca^{2+}$ in the cleft: fast and fluorescent. *Circ Res*. 2014;115:326–328. doi: 10.1161/CIRCRESAHA.114.304487.
55. Zhao YT, Valdivia HH. Ca2+ nanosparks: shining light on the dyadic cleft but missing the intensity of its signal. *Circ Res*. 2014;114:396–398. doi: 10.1161/CIRCRESAHA.113.303112.




## Novelty and Significance

### What Is Known?

- Global $Ca^{2+}$ release from the intracellular $Ca^{2+}$ store causes cardiac myocyte contraction.
- Localized $Ca^{2+}$ release such as $Ca^{2+}$ sparks often occur in diseased hearts, but whether the $Ca^{2+}$ spark can cause local sarcomere contraction was unresolved because of a lack of suitable technique.

### What New Information Does This Article Contribute?

- We developed a multimodal second harmonic generation and 2-photon fluorescence microscopy technique to simultaneously image the local $Ca^{2+}$ signal and sarcomere contraction at high spatiotemporal resolution.
- Our data show that $Ca^{2+}$ sparks can cause sarcomere contraction in subcellular microdomains (named myo-pinch), revealing a role for these events in generating subcellular strain during diastole.
- Local $Ca^{2+}$-contraction coupling is found altered in pressure-overload–induced heart failure, such changes in heart diseases can be studied by using the multimodal technique.

During the cardiac cycle, cardiac myocytes contract in systole to pump blood and relax in diastole to allow refilling. Systolic contraction is caused by a global release of $Ca^{2+}$ from the sarcoplasmic reticulum to increase cytosolic $Ca^{2+}$ concentration. Diastolic relaxation requires $Ca^{2+}$ to be sequestered into the sarcoplasmic reticulum and the cytosolic $Ca^{2+}$ concentration to be kept low. However, spontaneous $Ca^{2+}$ release from the sarcoplasmic reticulum can occur during diastole, especially in diseased hearts. Whether localized $Ca^{2+}$ release, in the form of $Ca^{2+}$ sparks, can cause local sarcomere contraction has been an important but unresolved issue. Here, we develop a multimodal second harmonic generation and 2-photon fluorescence imaging imaging method that uses second harmonic generation to monitor the contraction of individual sarcomeres and 2-photon fluorescence to image a fluorescent $Ca^{2+}$ indicator. This enables the simultaneous imaging of local $Ca^{2+}$ signals and sarcomere contraction at high spatiotemporal resolution. Our data reveal that $Ca^{2+}$ sparks can indeed cause sarcomere contractions in subcellular microdomains, which suggests that they increase mechanical stress within the cell during diastole. We also find that microdomain $Ca^{2+}$-contraction coupling is altered in pressure-overload–induced heart failure. Thus, the second harmonic generation and 2-photon fluorescence imaging technique enables the deciphering of disease-related changes in $Ca^{2+}$-contraction coupling at the single sarcomere level.

Circulation Research
JOURNAL OF THE AMERICAN HEART ASSOCIATION



# Multimodal SHG-2PF Imaging of Microdomain $Ca^{2+}$-Contraction Coupling in Live Cardiac Myocytes

Samir Awasthi, Leighton T. Izu, Ziliang Mao, Zhong Jian, Trevor Landas, Aaron Lerner, Rafael Shimkunas, Rahwa Woldeyesus, Julie Bossuyt, Brittani Wood, Yi-Je Chen, Dennis L. Matthews, Deborah K. Lieu, Nipavan Chiamvimonvat, Kit S. Lam, Ye Chen-Izu and James W. Chan

*Circ Res.* 2016;118:e19-e28; originally published online December 7, 2015;
doi: 10.1161/CIRCRESAHA.115.307919
*Circulation Research* is published by the American Heart Association, 7272 Greenville Avenue, Dallas, TX 75231

Print ISSN: 0009-7330. Online ISSN: 1524-4571

## SUPPLEMENTAL MATERIAL

### Detailed Methods

All laboratory procedures in this study conform to the *Guide for the Care and Use of Laboratory Animals* published by the US National Institutes of Health, the Guide for the Care and Use of Laboratory Animals laid out by Animal Care Committee of the University of California (UC). The animal use was approved by the UC Davis Institutional Animal Care and Use Committee.

***Cell isolation***

Sprague-Dawley rats were purchased from Charles River (http://www.criver.com). The rats were anesthetized with nembutal (100 mg/kg injected IP). After testing for the suppression of reflexes, the hearts were explanted via midline thoracotomy. A standard enzymatic technique was used to isolate the ventricle myocyte. Briefly, the heart was mounted on a Langendorff system and perfused with a modified Tyrode solution containing (in mmol/L) NaCl 135, KCl 4, MgSO4 1.0, $NaH_2PO_4$ 0.34, glucose 15, HEPES 10, taurine 10, pH 7.25 (adjusted with NaOH); the perfusion solution was pre-warmed to 37$^o$C and bubbled with 100% $O_2$. Then, collagenase B (~ 1 mg/ml, F. Hoffmann-La Roche Ltd, Switzerland), protease type XIV (~0.1 mg/ml), 0.1% BSA and 20 μM $Ca^{2+}$ were added into the perfusion solution, and the heart was enzymatically digested for 15-20 minute. The ventricular tissue was cut down and minced; the remaining tissue was further incubated in the enzyme solution at 37$^o$C for 15-45 minutes, and minced again to collect isolated ventricular myocytes. The cells were used for experiments within 6 hours after isolation.

***Cell preparation for Fluo-4 loading and Di8-ANNEPS staining in live cardiomyocytes***

Freshly isolated rat VCMs were incubated in $Ca^{2+}$ free Tyrode's solution containing: 145 mM NaCl, 4 mM KCl, 0.33 mM $NaH_2PO_4$, 1 mM $MgCl_2$, 10 mM HEPES, 10 mM glucose; the pH was adjusted to 7.3 with NaOH. Prior to imaging, the $Ca^{2+}$ concentration in the cell incubation solution was increased to 1 mM in a stepwise manner. The cells were consecutively incubated in Tyrode's solution with 0.2 mM, 0.5 mM and 1 mM $Ca^{2+}$ for 30 min, 20 min and 20 min respectively. The cells were loaded by incubating 0.5 ml of the cell suspension with 0.5 ml of a solution containing $Ca^{2+}$ indicator Fluo-4/AM 2.5 μM (Molecular Probes-Invitrogen, Carlsbad, CA) and 0.75 μM pluronic acid in Tyrode's solution with 1 mM $Ca^{2+}$, for 30 min at room temperature. To visualize T-tubules, the cells were incubated for 5 min in Tyrode's solution with 1 mM $Ca^{2+}$ and 5 μM Di8-ANEPPS (Molecular Probes-Invitrogen).

***Antibody labeling in fixed cardiomyocytes***

RyRs of mouse VCMs were labeled with Alexa Fluor 488 conjugated anti-$RyR_2$ antibodies. The cells were fixed in 1% paraformaldehyde for 5 min and washed in cold phosphate buffered saline (PBS) solution twice. Cell membranes were permeabilized by incubating with 0.1% Triton X-100 solution at RT for 5 min, washed, and blocked. After blocking, the cells were incubated with primary antibody (Anti-$RyR_2$, mouse monoclonal antibody, MA3-916, Affinity BioReagents, Golden, CO) for 2 hours at RT. They were washed twice with 0.01% Triton X-100 and incubated with secondary antibody (Alexa Fluor 488, Goat anti-mouse IgG, Molecular Probes) for another 2 hours at RT. Finally, the cells were washed twice with 0.01% Triton X-100 and re-suspended in PBS.

***Transverse aortic constriction (TAC) surgery and echocardiographic measurements***

TAC was performed on mouse (male, 11 week old) as described previously (Rockman et al, ref below), with some modifications. Briefly, after deep anesthesia was induced with 2-4% isoflurane, a small incision was made into the chest cavity in the second intercostal space. The transverse aorta was ligated with suture tied against a 27- gauge wire. Successful constriction of the aorta was confirmed through observation of diminished left carotid artery perfusion. Under 1-4% isoflurane anesthesia

echocardiographic measurements were taken two days before, and 2 weeks and 7 weeks after TAC surgery. Analysis was performed using a Visual Sonic Vevo 2100 system. After confirmation of a decrease of the ejection fraction to less than 50% after 7-8 weeks post TAC, the mouse was used for cardiomyocytes isolation and experimentation.

***Calculation of A-band distance pdf using the kernel density methods***

The histogram of A-bands distance (Fig.3C) is calculated using the kernel density methods.[36,37] For every measured distance $d_i$ between adjacent A-bands in the linescan image we define the function

$$h\left(x,d_i\right)=\frac{1}{\sqrt{2\pi}\,wN}\exp\left(-\frac{(x-d_i)^2}{2w^2}\right) \tag{0.1}$$

where $N$ is the total number of distances. $w$ is the bandwidth and, like bin widths used to construct histograms, larger values give smoother pdfs but can lead to loss of resolution. The estimate of the distance pdf $f(x)$ is

$$f(x)=\sum_{i=1}^{N}h(x,d_i)\ . \tag{0.2}$$

By construction, the integral of $f(x)$ overall $x$ is unity.

## Online Figure I

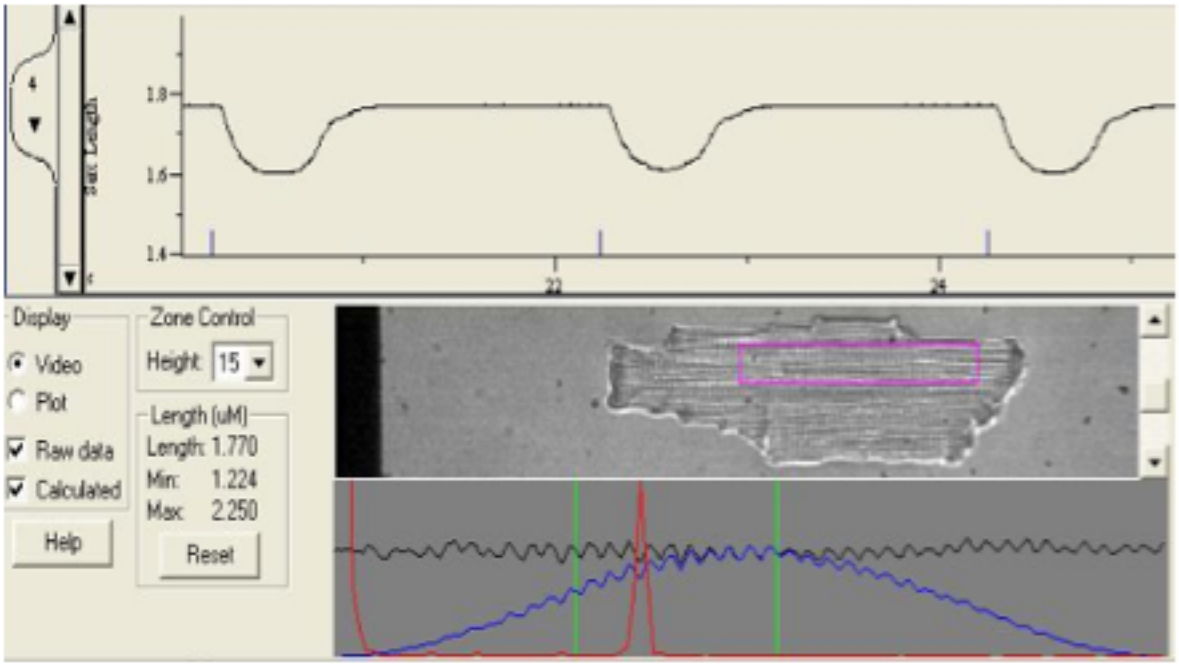


**Online Figure I.** Sarcomere length measurement using transmission image.
The rat ventricular myocyte shows clear striated sarcomere pattern in the transmission image (middle panel). This pattern in the region of interest (box in magenta color) is recorded as the the periodic change in the light intensity (lower panel, grey line), the FFT spectrum of which is used to calculate the sarcomere length. The change of sarcomere length during cell contraction (upper panel, Sarc Length) show the Sarc Length is about 1.8 μm in diastole and about 1.6 μm in systole.

## Online Figure II

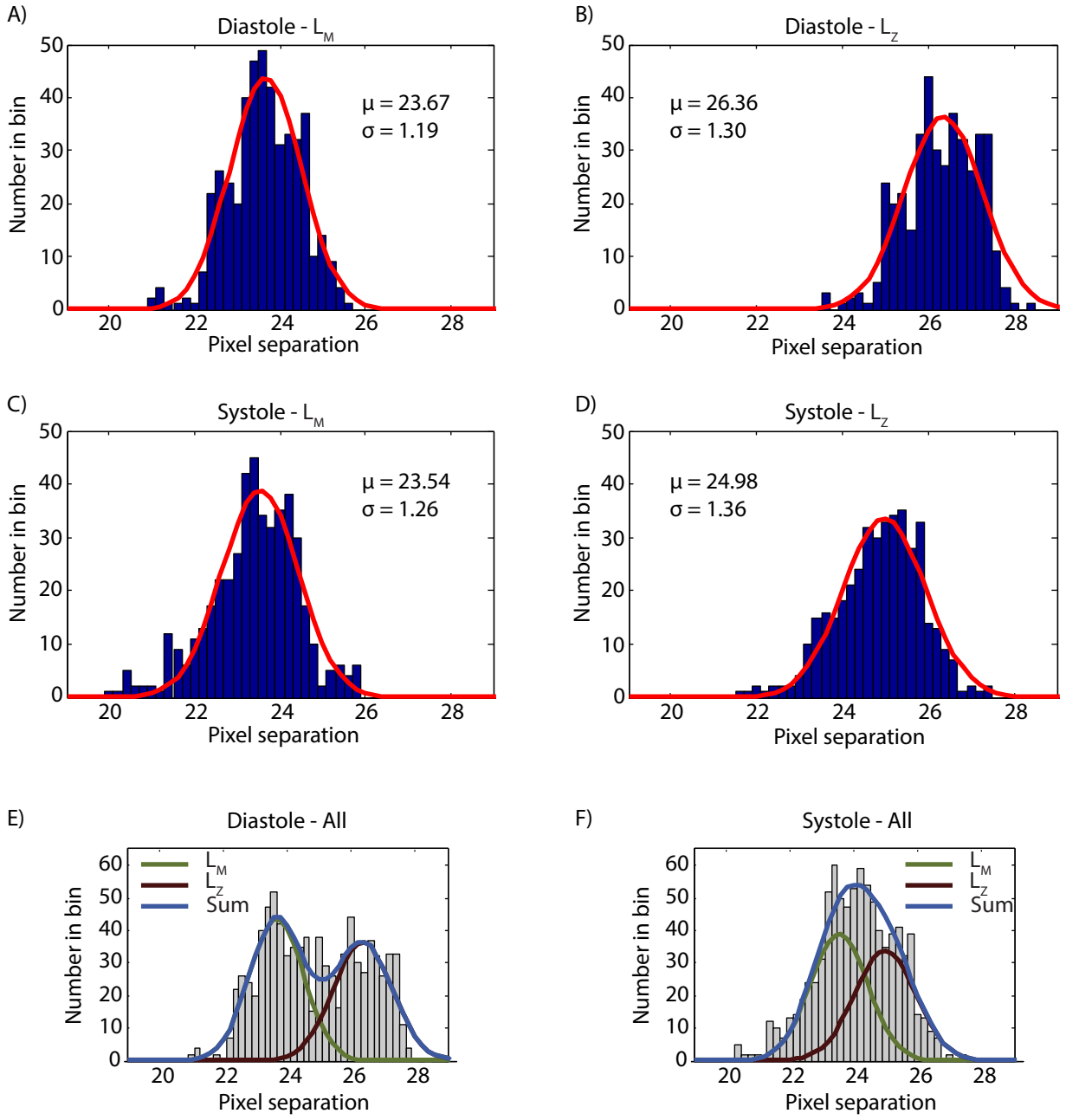


**Online Figure II.** Histograms of center-to-center distances from Figure 4 of the main text.
Following the data analysis procedure depicted in Figure 4 of the main text, the center-to-center distances between the SHG bright bands were determined and collected into histograms. Alternating distances were binned separately (A-D) and together (E-F) during diastole (A-B) and systole (C-D). Gaussian fits were performed on the histogram data. The alternating distances corresponding to $L_M$ did not shorten during contraction (A vs. C) whereas those corresponding to $L_Z$ did shorten (B vs. D). For Figures 4G-H of the main text (E and F above), all center-to-center distances were binned together (no separation of $L_M$ and $L_Z$), but the Gaussian fits from A-D above were displayed on the plots to show the relative contributions of $L_M$ and $L_Z$ to the histogram. the "sum" curve in E and F above shows the sum of the displayed Gaussian curve. In these figures, each pixel is approximately 0.033 microns.

## Online Figure III

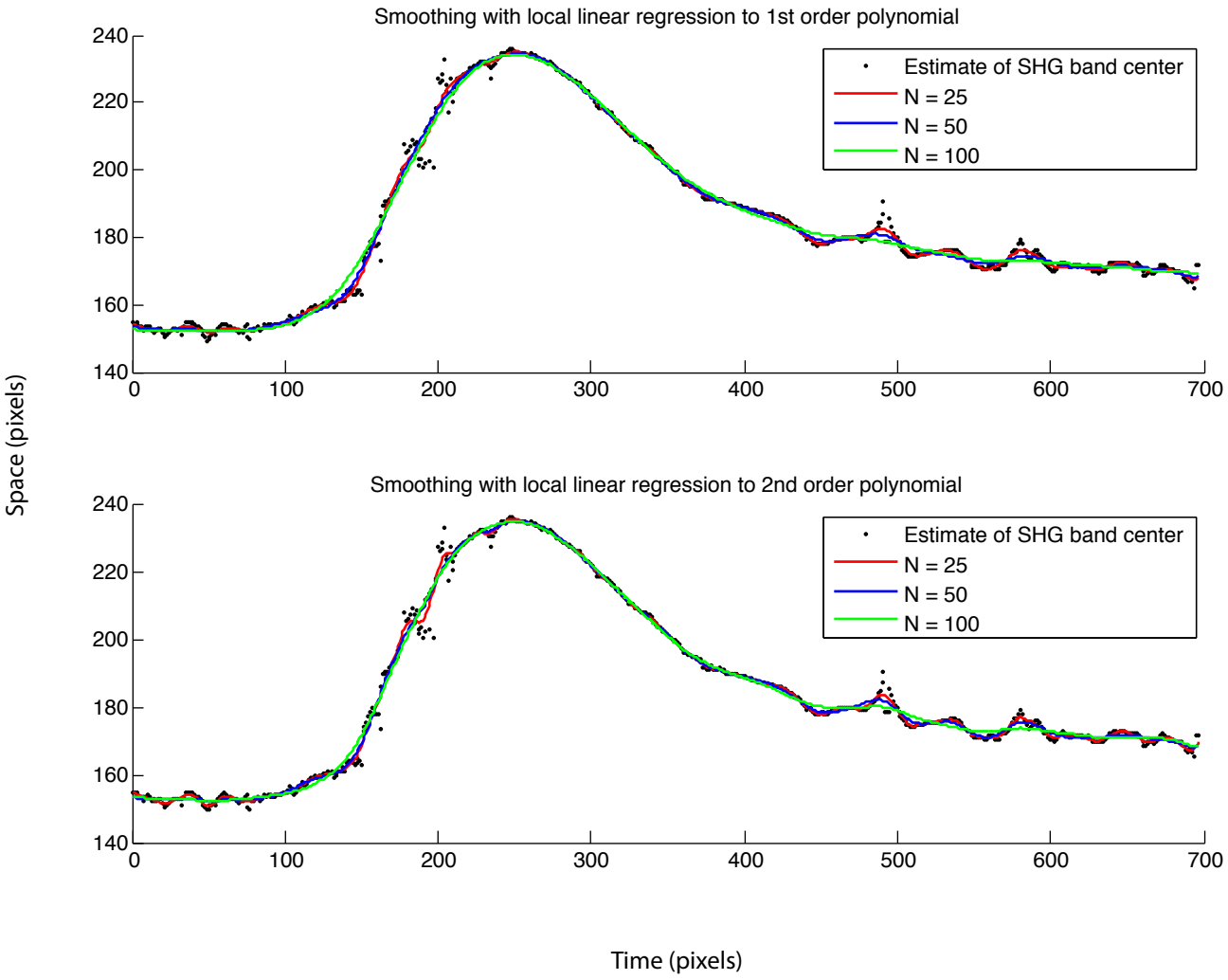


**Online Figure III.** Smoothing using a local linear regression.
We use a local linear regression to smooth data. In the process, a polynomial is fit to data in a window that is N pixels wide. The window is moved across the data set pixel by pixel. The resulting fits are averaged to obtain the smooth data set. The figure above shows the result of the smoothing process on a single SHG-bright band from the data in Figure 5B of the main text. The figure shows fits using different window sizes (N) and a first degree polynomial (top) or a second degree polynomial. The exact N necessary depends on the signal-to-noise ration in the raw data.

## Online Figure IV

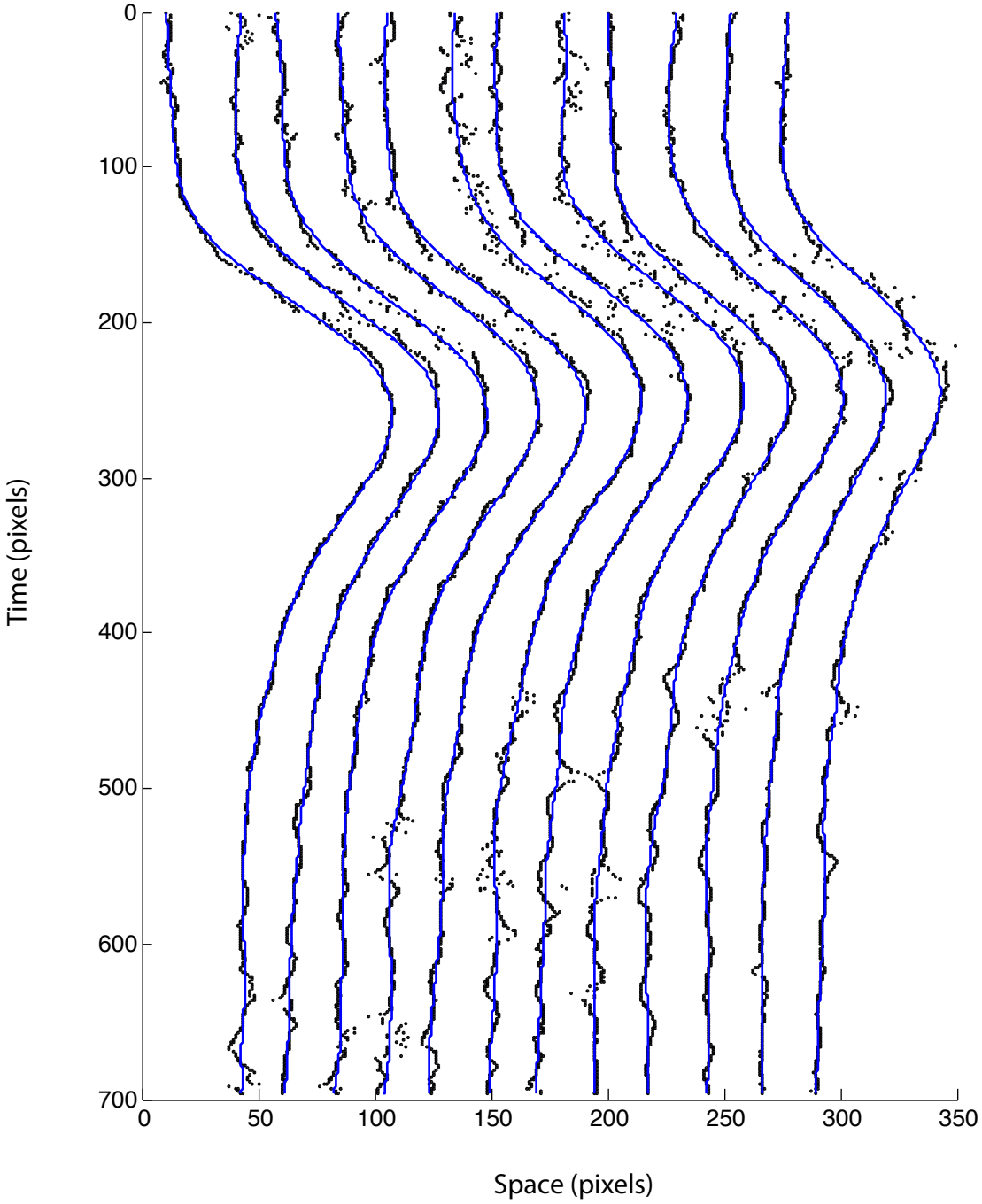


**Online Figure IV:** Smoothing process applied to a full calcium wave data set.
The result of applying the smoothing process from Online Figure III, using N = 100 and a first order polynomial, to the data used to generate Fig. 5B in the main text, is shown above.

## Online Figure V

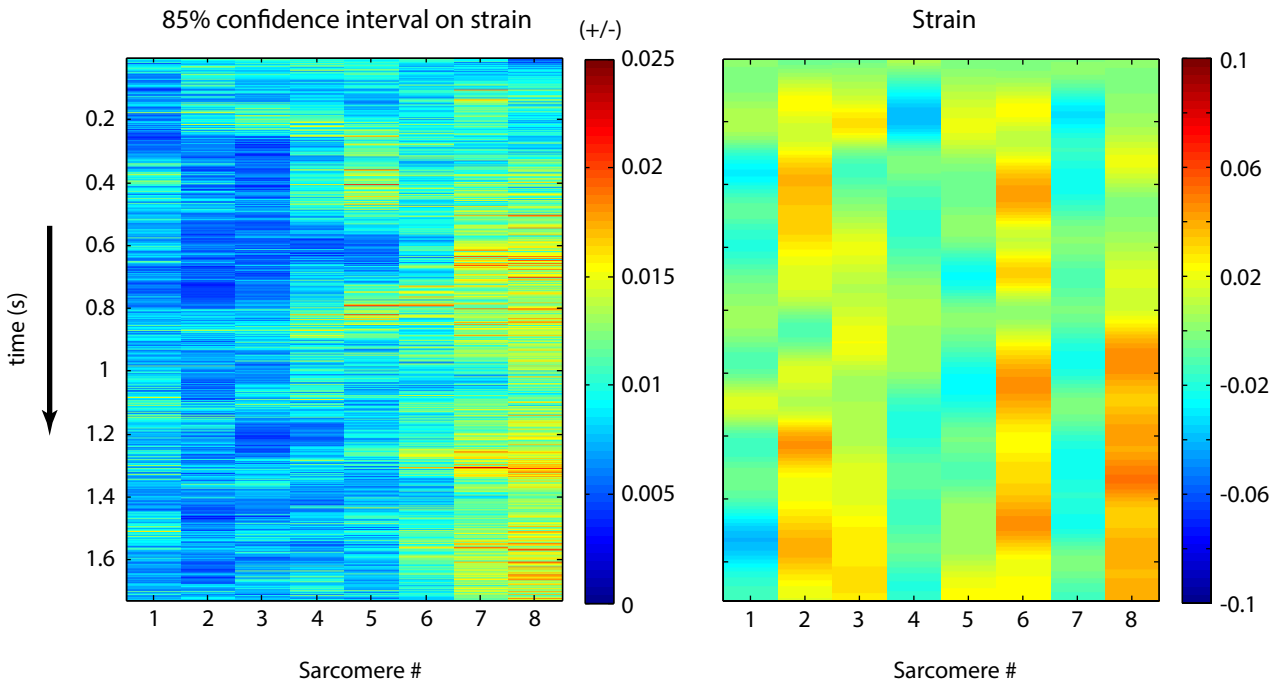


**Online Figure V:** 85% confidence intervals on peak-finding propagated through calculation of Ca(2+)-spark induced strain. 85% confidence intervals (CIs) were obtained from the Gaussian fitting algorithm (described in Fig. 4 of the main text) that was applied to the calcium spark data underlying Fig. 5C and Fig. 6B-C. The CIs were sub-pixel when displayed over the full set of peaks (e.g. Online Figure VI A). In order demonstrate the ultimate impact of the CIs, they were propagated through the calculation of strain in order to obtain 85% CIs on the local strain events. The CIs are displayed above in a heat map (left panel), next to the strain data (right panel). The CIs were calculated from data before smoothing, whereas the strain map is calculated from post-smoothing data, as described in the main text.

## Online Figure VI

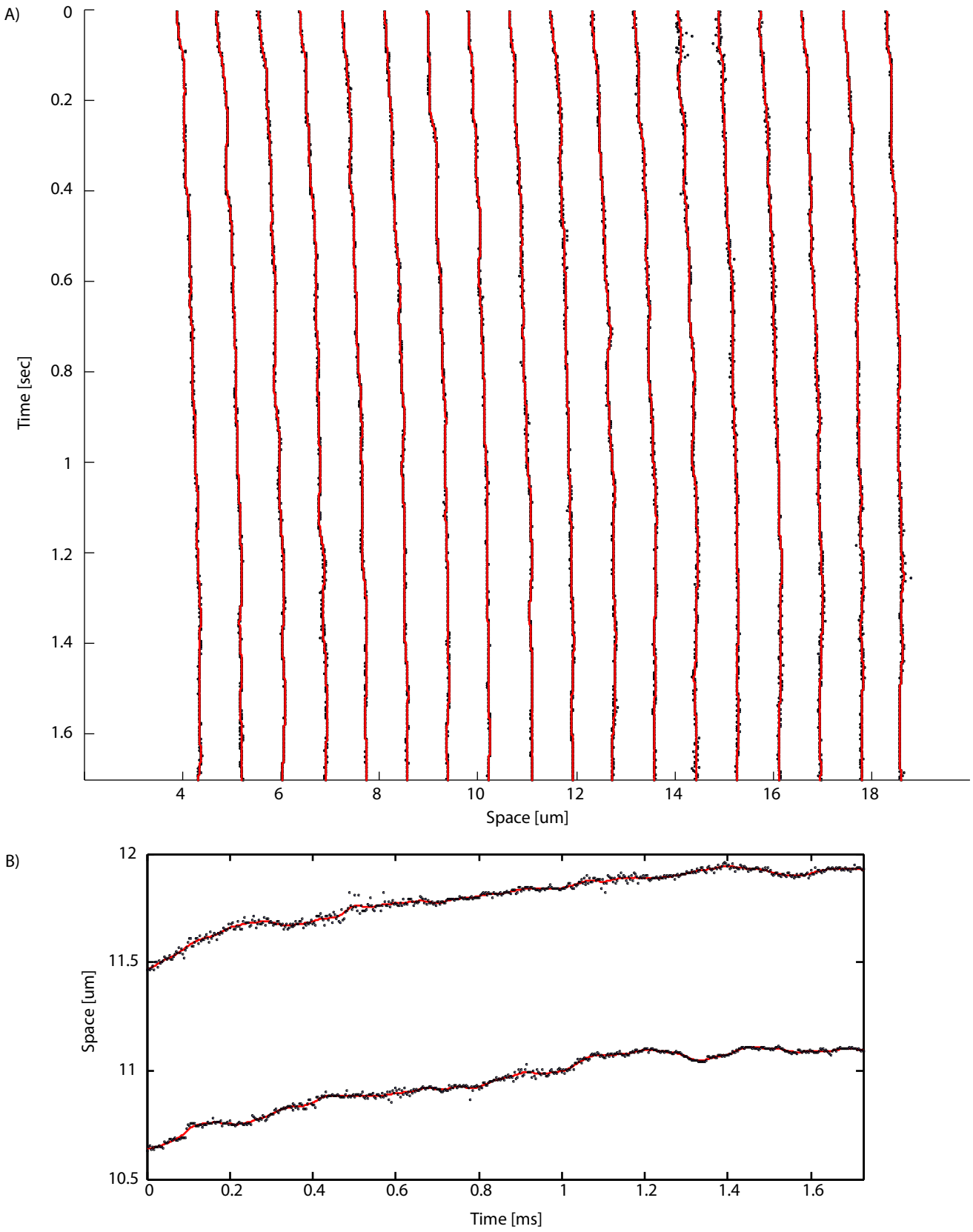


**Online Figure VI.** Smoothing applied to the calcium spark data set.
A) The result of applying the smoothing process from Online Figure III, using N = 20 and a first order polynomial, to the data used to generate Figure 5C in the main text, is shown above. B) Examples of individual bands from (A).

## Online Figure VII

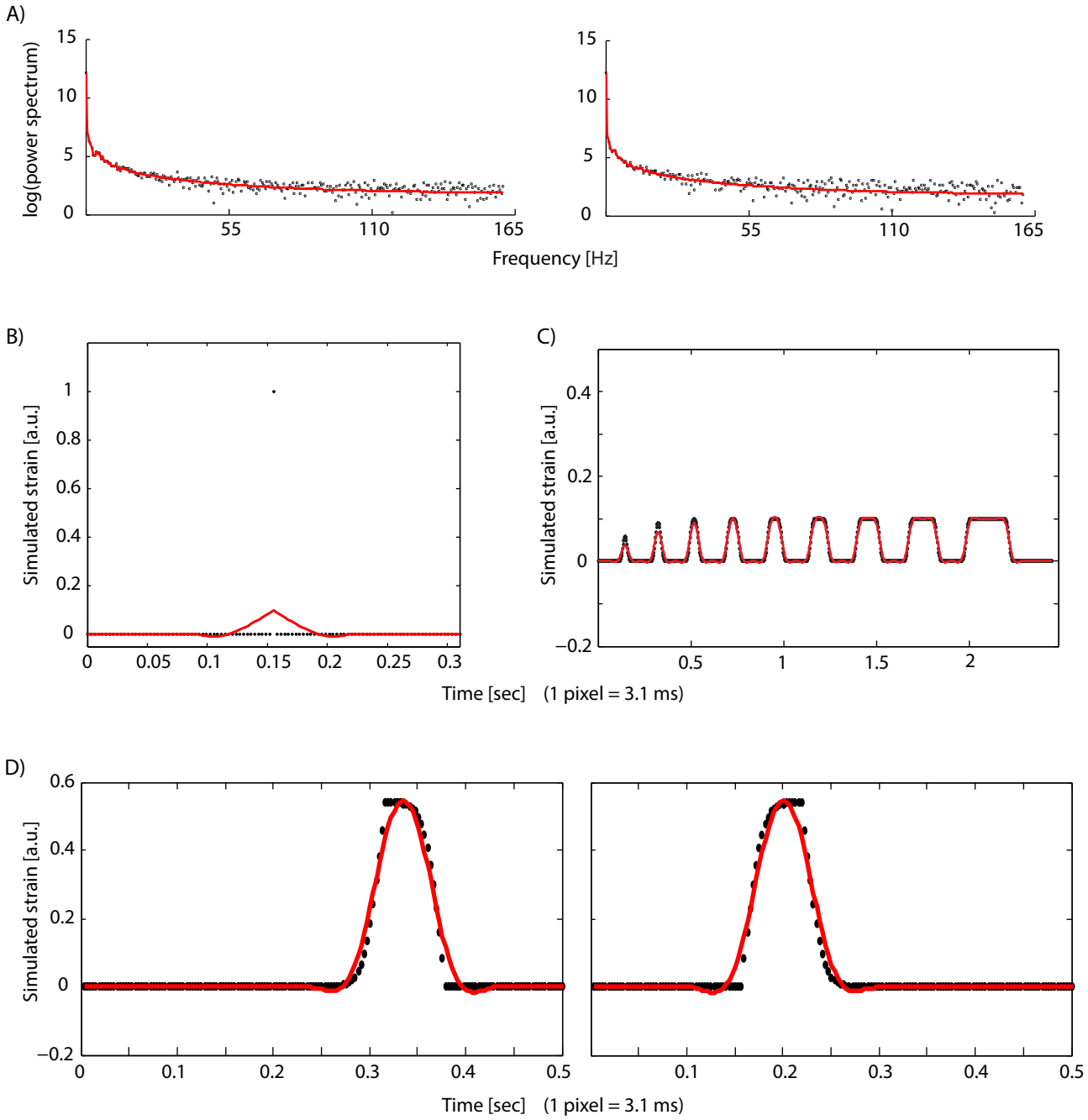


**Online Figure VII:** Effect of smoothing on calcium spark-induced strain.
A) Effect of smoothing on the power sepctra of the bands shown in Online Figure VI B, before (black dots) and after (red line). Smoothing significantly attenuates structure in the power spectra at frequencies of approximately 16-17 Hz and higher. B) Effect of smoothing on a delta function of strain in time (time resolution is 3.1 ms/pixel, as in raw SHG linescan data). C) Effect of smoothing on various smoothed step functions of strain. Smoothing significantly attenuates strain events lasting 60-70 ms and less. D) Simulated strain events with rapid onset/recovery and asymmetry in contraction or relaxation (black dots) were smoothed using the local linear regression algorithm (n=20 pixels, or ~ 60 ms) discussed in the text. Contractile events with fast rise/relaxation times and sharp transitions may be blurred and delayed by the smoothing process. In all plots above, black dots represent data before smoothing algorithm, and red lines represent smoothed data.